ISSN 1070-3284, Russian Journal of Coordination Chemistry, 2023, Vol. 49, No. 10, pp. 688–693. © Pleiades Publishing, Ltd., 2023.
Russian Text © The Author(s), 2023, published in Koordinatsionnaya Khimiya, 2023, Vol. 49, No. 10, pp. 659–664.

Interaction of Cobalt Tetrasulfophthalocyanine with ORF8 Accessory Protein of SARS-CoV-2

O. I. Koifman[a, b], V. E. Maizlish[b], N. Sh. Lebedeva[a], E. S. Yurina[a], S. S. Guseinov[a], E. L. Guriev[c], and Yu. A. Gubarev[a, *]

[a] *G.A. Krestov Institute of Solution Chemistry of the Russian Academy of Sciences, Ivanovo, Russia*
[b] *Ivanovo State University of Chemical Technology, Ivanovo, Russia*
[c] *Lobachevsky State University of Nizhny Novgorod, Nizhny Novgorod, Russia*
**e-mail: gua@isc-ras.ru*

Received January 19, 2023; revised March 13, 2023; accepted March 22, 2023

Abstract—The interaction of cobalt(II) tetrasulfophthalocyanine (CoPc) with the ORF8 accessory protein of SARS-CoV-2 was studied by spectroscopy and calorimetry. The protein was found to shift the aggregation equilibrium in cobalt tetrasulfophthalocyanine solutions towards dimerization. Most probably, the CoPc dimer binds to ORF8 on the greater β-sheet side, thus causing fluorescence quenching. The protein affinity constant to CoPc dimer is 1.5×10^5. Differential scanning calorimetry data indicate that ORF8 undergoes thermally induced denaturation in the temperature range of 38–67°C. Melting of ORF8 includes two stages, which partly overlap. The complex formation of ORF8 with CoPc leads to thermal stabilization of the protein, thus preventing the second stage of protein unfolding. Denaturation of the complex proceeds between 40 and 77°C as two temperature-separated stages. According to gel electrophoresis and immunoblotting data, visible light photoirradiation of the ORF8 complex with CoPc does not induce photooxidation of the protein. It was shown that water-soluble cobalt sulfo-substituted phthalocyanine can be considered as a potential drug inhibiting the ORF8 accessory protein.

Keywords: SARS-CoV-2, metal phthalocyanines, protein, complex, photoinactivation

DOI: 10.1134/S1070328423600481

INTRODUCTION

The COVID-19 disease caused by the SARS-CoV-2 virus, which appeared in China, has rapidly spread around the world and still causes enormous economic and social damage. To date, this coronaviral infection caused death of more than 6.7 million patients. One of the most frequent causes of the lethal outcome is cytokine storm, the appearance and development of which involves the accessory proteins of SARS-CoV-2, such as ORF8, ORF10, and ORF3a. Currently, there are no drugs targeting the accessory proteins of SARS-CoV-2 and approved for use. According to the existing protocols, the cytokine storm is treated with a combination of remdesivir with dexamethasone. Dexamethasone is an immunomodulating agent, but its efficacy against the cytokine storm is quite disputable. For example, according to [1], the mortality among patients who received dexamethasone together with remdesivir was 16.7%, while in the case of remdesivir combined with tocilizumab it was 5.3%. However, there are also data about successful use of dexamethasone together with remdesivir [2]: the 30-day mortality among patients who received remdesivir and dexamethasone in addition to SOC (standard of care) was 12.6% versus 19.7% for those who received only SOC. Therefore, the search for compounds able to inhibit or inactivate the accessory proteins of SARS-CoV-2, which modulate the immune response of the host and initiate the cytokine storm, is a relevant task. Macrocyclic compounds are potentially suitable for inhibition and inactivation of viruses [3, 4]. Our previous studies demonstrated that macroheterocyclic compounds form stable complexes with SARS-CoV-2 accessory proteins. Particularly, the ORF8 [5], ORF3a [6, 7], and ORF10 [8] proteins are inhibited by 5,10,15,20-tetrakis(N-methyl-3-pyridyl)chlorin. A more promising method is photoinactivation of the protein. Under the action of light, porphyrin, chlorin, and phthalocyanine macroheterocycles can generate reactive oxygen species, which oxidize the amino acid residues of the protein and thus irreversibly damage its structure and functions [3, 4, 9]. Regarding ORF3a and ORF10 accessory proteins, we showed previously that they are photoinactivated when complexed with cobalt(II) tetrasulfophthalocyanine. The efficiency of inhibition/photoinactivation of the ORF8 protein of SARS-CoV-2 using cobalt(II) tetrasulfophthalocyanine (CoPc) has not been studied.

The purpose of this study was to evaluate the photocatalytic activity and the inhibiting properties of CoPc against the ORF8 accessory protein of SARS-CoV-2.

EXPERIMENTAL

The compound CoPc was prepared by the urea fusion method [10, 11]. The melt was ground and dissolved in water, the solution was filtered, and the filtrate was evaporated. The product was washed with concentrated hydrochloric acid until the filtrates were colorless and dried. The product was dissolved in water, and the aqueous solution was passed through a column with the KU-2-8 cation exchange resin and chromatographed successively on silica gel and molselect G-10, while collecting the most colored zone. The resulting solution was evaporated, and the dry product was treated with organic solvents (methanol, acetone, benzene) in a Soxhlet apparatus. The product was dried under vacuum at 100–110°C. The purity of CoPc was at least 98%.

Solutions were prepared using doubly distilled water and phosphate-buffered saline (PBS) with pH 7.4.

For $C_{32}H_{16}NO_{12}S_4Co$				
Anal. calcd., %	C, 43.1	H, 1.8	N, 12.6	S, 14.4
Found, %	C, 42.5	H, 1.9	N, 12.3	S, 14.2

The UV–Vis spectrum (DMSO; λ_{max}, nm (logε)): 664(5.15), 602(4.50), 330(4.85) coincides with published data [12].

ORF10 was expressed in *E. coli* BL21(DE3) cells based on pGBW-m4046950, kindly provided by Ginkgo Bioworks & Benjie Chen (Addgene 149258 plasmid; http://n2t.net/addgene:149258; RRID: Addgene_149258). The procedure was described in detail in [6]. The molecular mass and identity of the target proteins was confirmed by polyacrylamide gel (PAAG) electrophoresis and immunoblotting.

The absorption spectra and fluorescence spectra were recorded on an AvaSpec-2048 spectrophotometer (Avantes BV, the Netherlands) in 10 mm cells in a temperature-controlled cell at 25°C.

The thermochemical measurements were performed on a DSC 204 F1 heat flux differential scanning calorimeter (DSC) (Netzsch Geratebau GmbH, Germany). Samples (solutions) weighing 10–15 mg were placed into pressed aluminum crucibles. An empty aluminum crucible served as the reference. The calorimetric experiment was carried out in a dynamic dry argon atmosphere (99.998% argon content) at a flow rate of 40 mL min^{-1} and a heating rate of 1°C min^{-1} in the temperature range of 12–93°C. The results were referred to the baseline obtained for two empty crucibles. The temperature and sensitivity of the calorimeter were calibrated by measuring phase transition temperatures and enthalpies for 11 standard substances: Hg, C_6H_{12}, $C_{12}H_{10}$, KNO_3, $RbNO_3$, In, Bi, Sn, Zn, $KClO_4$, and CsCl. The accuracy of temperature measurements was 0.3°C and the accuracy of weighing was 0.01 mg (Sartorius M2P Balance). The specific heat capacity of protein solutions was determined using the baseline, standard, and sample DSC curves. Sapphire served as the standard. All three measurements were successively performed within one day. Using the software for DSC 204 F1 Phoenix and experimental temperature dependences of the specific heat capacity of the standard (sapphire), we obtained the temperature dependences of the specific heat capacities of a protein solution and pure buffer. The difference between the heat capacities of the protein solution in the buffer and the pure buffer was found using the Origin software. Using the temperature dependence of the specific heat capacities after subtraction of the sigmoidal baseline, the positions of peaks were found.

Samples for electrophoresis and immunoblotting were prepared by mixing ORF8 with CoPc in 1 : 1 molar ratio in PBS. The mixture was incubated for 1 h in the dark or on exposure to a white light (10 W power). The samples were mixed in 4 : 1 volume ratio with 5× buffer (0.3 M Tris-OH pH 6.8, 10% SDS, 25% mercaptoethanol, 50% glycerol, 0.005% bromphenol blue), and electrophoresis was carried out in 12% polyacrylamide gel (TGX Stain-Free™ FastCast™ Acrylamide Kit 12%, Bio-Rad, USA). The gel images were obtained using a stain-free imaging technique in the ChemiDoc system (Bio-Rad, USA). In the case of ORF10, electrophoresis was carried out in 15% polyacrylamide gel, which was then stained with a coomassie blue R-250 solution (Thermo, USA).

The proteins were transferred from the gel to an Immobilon-P polyvinylidene fluoride membrane (Merck, Germany) using the Trans-Blot Turbo semi-dry transfer system (Bio-Rad, USA). The membrane was blocked for 1 h with a 5% solution of dry milk in TBS-T buffer (20 mM Tris, 150 mM NaCl, 0.05% Tween-20, pH 7.5). Then the membrane was incubated for 1 h in a 1 : 500 solution of primary antibodies (Rabbit Polyclonal SARS-CoV-2 ORF8 Antibody, FabGenix, USA) in 5% dry milk and TBS-T buffer. The membrane was washed three times with TBS-T buffer for 5 min, incubated for 1 h in a 1 : 10000 solution of secondary antibodies (Goat Anti-Rabbit IgG H&L HRP, Abcam, UK) in 5% dry milk in TBS-T, and washed as described above. The membrane was incubated for 5 min in a solution of peroxidase substrate (Clarity Western ECL Substrate, Bio-Rad, USA) and visualized using the ChemiDoc system.

The molecular docking was performed in the AutoDock Vina 1.1.2 program [13] and visualized using PyMol 2.4.1. The structure of ORF8 D-I-Tasser (QHD43422.pdb) was uploaded in the website of

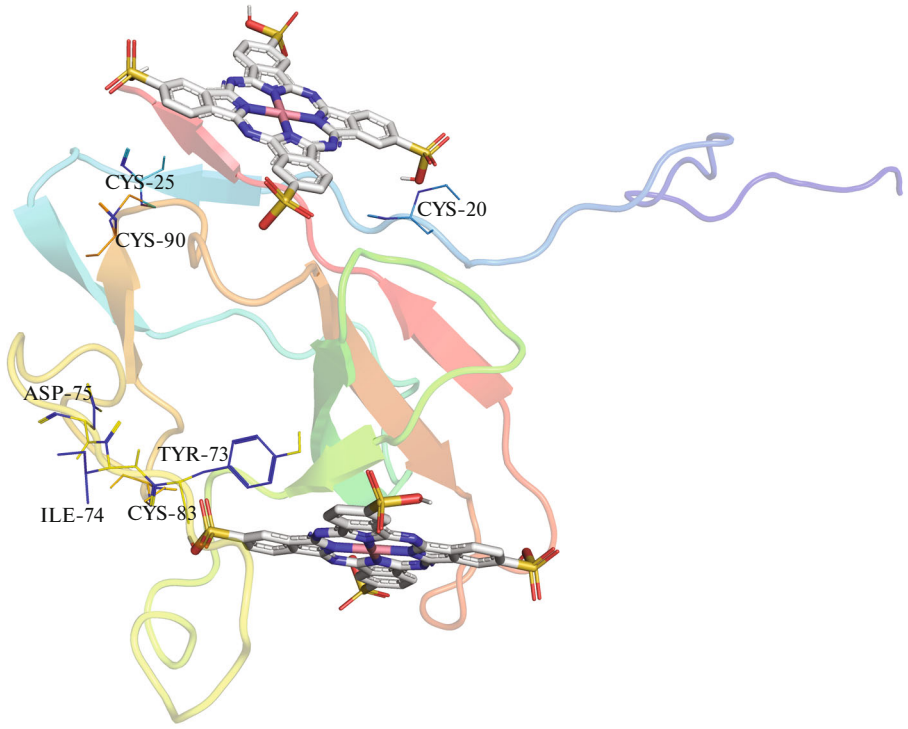

Fig. 1. Results of molecular docking of the ORF8 accessory protein of SARS-CoV-2 with CoPc.

Zheng's laboratory [14, 15]. The CoPc structure was minimized using ORCA 4.0 [16] by means of DFT methods. The surface charge of the protein globule was calculated using the Poisson–Boltzmann equation in order to eliminate the binding sites that cannot form bonds due to the electrostatic repulsion [17].

RESULTS AND DISCUSSION

The choice of water-soluble cobalt(II) phthalocyanine as a potential inhibitor and inactivator is due to the activity of this metal phthalocyanine against other accessory proteins of SARS-CoV-2 and also to the probable location of CoPc in the complex with ORF8 (Fig. 1). According to the molecular docking results, CoPc can bind to ORF8 with a relatively high energy (8.2–8.7 kcal/mol) in two ways (Fig. 1). One CoPc molecule is located in ORF8 near the amino acid sequence 73–75, responsible for ORF8 aggregation and binding to the major histocompatibility complex **I** (MHC-I), thus preventing viral antigen exposure on the cell surface induced by MHC-I [18]. The second CoPc molecule is located in the close vicinity of the N-terminal group of the protein responsible for the incorporation into the endoplasmic reticulum, thus suppressing the production of β-interferons [19]. One more benefit is the proximate position of a photo-vulnerable amino acid residue, cysteine, which occupies positions 20, 25, 83, and 90 in the ORF8 polypeptide chain. Note that, according to theoretical data, CoPc does not form axial bonds with electron-donating atoms of the protein, which is also a necessary condition for the use of a macroheterocyclic compound for photoinactivation [20].

Earlier, the ORF8 recombinant protein was spectrally characterized [5]; the presence of intrinsic fluorescence of the protein with a maximum at 345 nm enabled direct fluorescence titration of protein solutions with CoPc (Fig. 2). Titration of the ORF8 accessory protein with a CoPc solution results in quenching of the protein fluorescence. Processing of the results of spectral titration using the Scatchard approximation showed a fairly high affinity to ORF8; the Scatchard constant was 1.5×10^5. The Scatchard plot was linear ($R^2 = 0.988$); hence ORF8 binds to CoPc in only one possible way. It is noteworthy that in the initial phosphate buffer solution, CoPc is partly dimerized, as evidenced by the presence of absorption at 630 nm (Fig. 3) [21]. The reverse titration of CoPc solutions with a protein solution monitored by UV–Vis spectroscopy showed that an increase in the ORF8 content in the solution leads to decreasing 650/630 nm ratio of absorbances. This indicates that the protein initiates dimerization of the macroheterocyclic molecules. Thus, considering the data of direct and reverse titration indicates that CoPc binds to the protein in the dimeric form.

More information on the interaction of CoPc with ORF8 can be gained from DSC data. Figure 4 shows the temperature dependences of excess specific heat

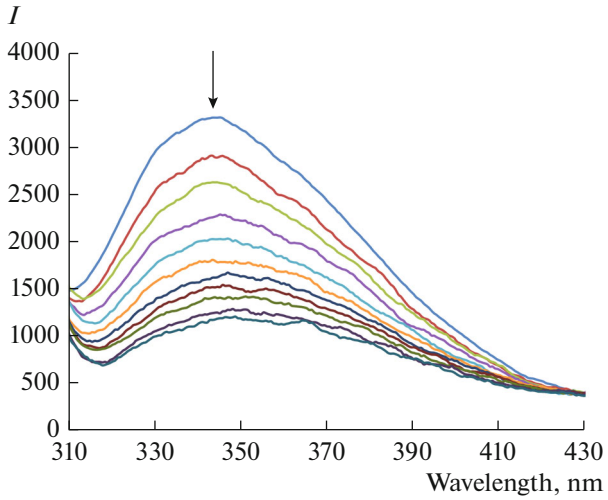

Fig. 2. Fluorescence spectra of ORF8 (2.24×10^{-5} M) during titration with CoPc (0–2.2×10^{-5} M) in PBS (pH 7.4).

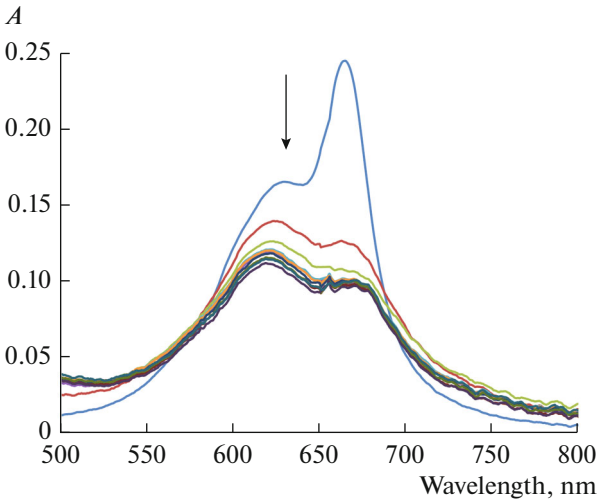

Fig. 3. UV–Vis spectra of CoPc (1.1×10^{-5} M) during titration with ORF8 (0–1.12×10^{-5} M) in PBS (pH 7.4).

capacities of solutions of ORF8 and its complex with CoPc before and after irradiation. It can be seen from Fig. 4 that the specific heat capacity of ORF8 solutions follows an intricate dependence. In the initial stage, an endotherm is present with a peak at 32.6°C; starting from 45°C, the excess heat capacity of the ORF8 solution increases non-linearly. The increase in the heat capacity reflects the increase in the degrees of freedom and intensity of molecular motions of the protein. It is clear that vibrational mobility of larger parts of the polypeptide chain appears with temperature rise. This enables conformational transitions of the protein associated with destruction of the native structure and additional hydration of amino acid residues that were isolated earlier in the folded structure. As can be seen from the dependence (Fig. 4), protein unfolding occurs in two stages, which give rise to two maxima in the excess heat capacity curve (47–48 and 57.6°C). The ORF8 core contains two antiparallel β-sheets. The smaller sheet consists of β2, β5, and β6, while the greater one consists of β3, β4, β7, and β8 [22]. Owing to this structure ORF8 can strongly inhibit type I interferon (IFN-β), ISRE interferon, and a NF-κB-responsive promoter [19]. The obtained thermochemical data suggest that the first peak in Fig. 4 (47–48°C) is associated with the disruption of β-folding of the smaller sheet, while the greater sheet is unfolded at 57.6°C. Further decrease in the heat capacity of the solutions is obviously attributable to the aggregation of ORF8 polypeptide chains after protein denaturation.

Binding of ORF8 to CoPc dimers changes the specific heat capacity curve both at low and at high temperatures; the first extremum with a maximum at 36.6°C is exothermic and may be related to structuring taking place in the system. This may be caused by decreasing electrostatic repulsion between oppositely charged CoPc groups and the amino acid residues of the polypeptide chain. The thermal denaturation of ORF8 complex with CoPc dimers, like that of single ORF8, proceeds in two stages. However, for the complex these stages are temperature-separated. The first endotherm has a maximum at the same temperature as the pure protein (47.6°C). The second endothermic effect observed for the ORF8–CoPc complex is shifted to higher temperature compared to that of ORF8; the temperature of the peak is 68°C. It is evident that the CoPc dimers stabilize the ORF8 protein by preventing the second stage of protein unfolding. If

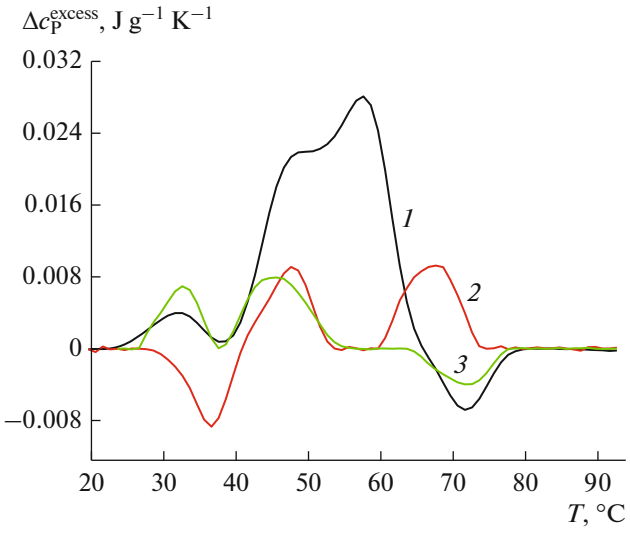

Fig. 4. Temperature dependences of excess specific heat capacities of solutions of (*1*) ORF8 and (*2, 3*) ORF8–CoPc complex (*2*) before and (*3*) after irradiation.

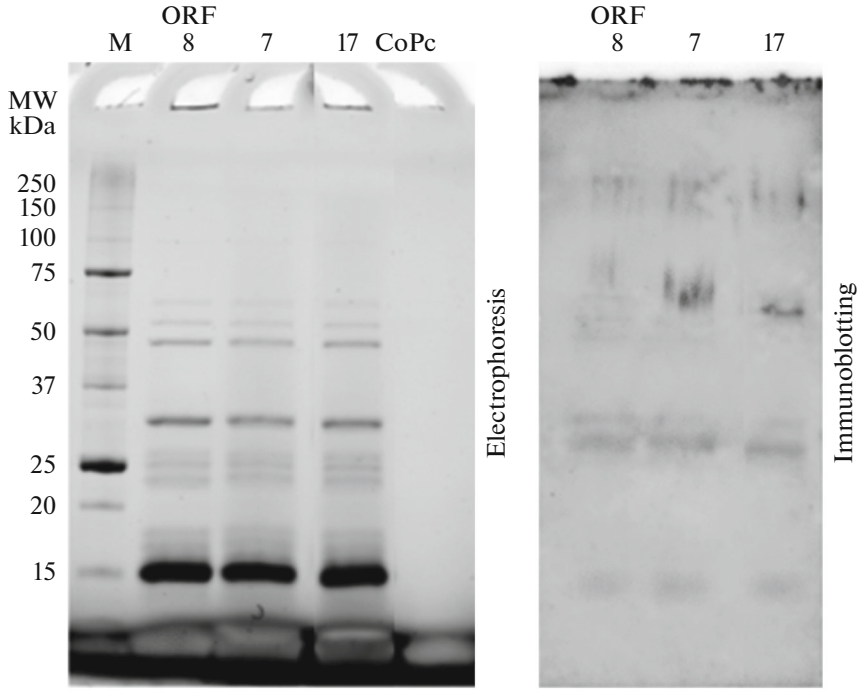

Fig. 5. Electrophoresis and immunoblotting results of ORF8 protein before and after incubation with CoPc: M are molecular weight markers; ORF8 is pristine protein; (7) ORF8 + CoPc; (17) ORF8 + CoPc + $h\nu$.

our assumption about the sequence of ORF8 thermal destruction is correct, it is likely that the CoPc dimers are located on the side of the greater β-sheet. It is of interest that the subsequent high-temperature exotherm is not manifested in the case of ORF8–CoPc complex.

The next goal of the study was to evaluate the effect of visible light (400–700 nm, 10 W, 1 h) on the complex of CoPc dimers with ORF8. Irradiation of the solutions significantly affected the pattern of excess heat capacity curve. The shape of the curve for the irradiated ORF8–CoPc complex almost completely coincides with the temperature dependence of the excess heat capacity of free ORF8, except for the second stage of protein unfolding, which is not detected in this case. Apparently, photoirradiation induces minor local changes in ORF8, the thermal denaturation of which occurs in one stage, and the complex probably dissociates during irradiation. To gain additional information on the effect of photoirradiation on solutions of ORF8–CoPc, we studied the pristine ORF8 and CoPc and their complexes before and after irradiation by electrophoresis and immunoblotting techniques (Fig. 5). In the lower part of the gel near the electrophoresis front, CoPc was detected. The incubation of ORF8 with CoPc in the dark (Fig. 5, lane 7) and under irradiation (Fig. 5, lane 17) did not change the pattern of electrophoresis and immunoblotting. The results confirm the conclusion made from analysis of DSC data on the absence of photocatalytic activity of CoPc towards ORF8. A possible cause for the low photocatalytic activity of CoPc in ORF8 oxidation is the dimerization of CoPc, which decreases the quantum yield of singlet oxygen.

SARS-CoV-2 developed several mechanisms to evade the host immune system such as ORF8-mediated downregulation of MHC-I and inhibition of β-interferon production. Our study demonstrated that the interaction of water-soluble cobalt tetrasulfo-substituted phthalocyanine with the ORF8 protein results in dimerization of CoPc. Cobalt sulfonated phthalocyanine dimers bind to the accessory protein of SARS-CoV-2, apparently, in the region of the greater β-sheet, which may facilitate restoration of the adaptive immunity during the SARS-CoV-2 infection. Because of the dimerization, it is inexpedient to consider CoPc as a photosensitizer for the photooxidation of SARS-CoV-2 ORF8, as in the dimerized state it has a low photocatalytic activity.

FUNDING

This study was supported by the Russian Science Foundation (grant no. 21-73-20140).

CONFLICT OF INTEREST

The authors of this work declare that they have no conflicts of interest.

REFERENCES

1. Garcia-Vidal, C., Meira, F., Cózar-Llistó, A., et al., *Rev. Esp. Quimioter.*, 2021, vol. 34, p. 136. https://doi.org/10.37201/req/018.2021
2. Benfield, T., Bodilsen, J., Brieghel, C., et al., *Clin. Infect. D*, 2021, vol. 73, p. 2031. https://doi.org/10.1093/cid/ciab536
3. Koifman, O., Ageeva, T., and Kuzmina, N.S., *Macroheterocycles*, 2022, vol. 15, p. 207. https://doi.org/10.6060/mhc224870k
4. Lebedeva, N.S., Gubarev, Y.A., Koifman, M.O., et al., *Molecules*, 2020, vol. 25, p. 4368. https://doi.org/10.3390/molecules25194368
5. Gubarev, Y.A., Lebedeva, N.S., Yurina, E.S., et al., *J. Biomol. Struct. Dyn.*, 2022, p. 1. https://doi.org/10.1080/07391102.2022.2079562
6. Lebedeva, N.S., Gubarev, Y.A., Mamardashvili, G.M., et al., *Sci. Reports*, 2021, vol. 11, p. 1. https://doi.org/10.1038/s41598-021-99072-8
7. Koifman, O.I., Lebedeva, N.S., Gubarev, Y.A., et al., *Chem. Heterocycl. Compd.*, 2021, vol. 57, p. 423. https://doi.org/10.1007/s10593-021-02920-8
8. Koifman, M.O., Malyasova, A.S., Romanenko, Y.V., et al., *Spectrochim. Acta, Part A*, 2022, vol. 279, p. 121403. https://doi.org/https://doi.org/10.1016/j.saa.2022.121403
9. Koifman, O.I., Ageeva, T.A., Beletskaya, I.P., et al., *Macroheterocycles*, 2020, vol. 13, p. 311. https://doi.org/10.6060/mhc200814k
10. Weber, J.H. and Busch, D.H., *Inorg. Chem.*, 1965, vol. 4, p. 469. https://doi.org/10.1021/ic50026a007
11. Shaposhnikov, G., Kulinich, V., and Maizlish, V., *Modifitsirovannye ftalotsianiny i ikh strukturnye analogi* (Modified Phthalocyanines and Their Structural Analogues), Moscow: Krasand, 2012.
12. Maizlish, V., Mochalova, N., Snegireva, F., et al., *Izv. Vyssh. Uchebn. Zaved. Khim. Khim. Tekhnol.*, 1986, vol. 29, p. 3.
13. Trott, O. and Olson, A.J., *J. Comput. Chem.*, 2010, vol. 31, p. 455. https://doi.org/10.1002/jcc.21334
14. Zhang, C., Zheng, W., Huang, X., et al., *J. Proteome Res.*, 2020, vol. 19, p. 1351. https://doi.org/10.1021/acs.jproteome.0c00129
15. Zheng, W., Zhang, C., Li, Y., et al., *Cell Rep. Methods*, 2021, p. 100014. https://doi.org/10.1016/j.crmeth.2021.100014
16. Neese, F., *Wiley Interdiscip. Rev. Comput. Mol. Sci.*, 2022, vol. 12, p. e1606. https://doi.org/10.1002/wcms.1606
17. Baker, N.A., Sept, D., Joseph, S., et al., *Proc. Natl. Acad. Sci. U. S. A.*, 2001, vol. 98, p. 10037. https://doi.org/10.1073/pnas.181342398
18. Zhang, Y., Chen, Y., Li, Y., et al., *Proc. Natl. Acad. Sci. U. S. A.*, 2021, vol. 118, p. e2024202118. https://doi.org/10.1073/pnas.2024202118
19. Li, J.-Y., Liao, C.-H., Wang, Q., et al., *Virus Res.*, 2020, vol. 286, p. 198074. https://doi.org/10.1016/j.virusres.2020.198074
20. Lebedeva, N.S., Yurina, E.S., Gubarev, Y.A., et al., *J. Photochem. Photobiol., A*, 2018, vol. 353, p. 299. https://doi.org/10.1016/j.jphotochem.2017.11.037
21. Lebedeva, N.S., Popova, T., Mal'kova, E., et al., *Russ. J. Phys. Chem. A*, 2013, vol. 87, p. 2030. https://doi.org/10.1134/S0036024413120133
22. Flower, T.G., Buffalo, C.Z., Hooy, R.M., et al., *Proc. Natl. Acad. Sci. U. S. A.*, 2021, vol. 118, p. e2021785118. https://doi.org/10.1073/pnas.2021785118

Translated by Z. Svitanko